International Journal of Trend in Research and Development, Volume 11(3), ISSN: 2394-9333
www.ijtrd.com

Simulation of $Cusn_{12}ni_2$ Alloy Melt Pool on the Surface of 20 Steel Pipes by Laser Cladding

[1]Xue Yongheng and [2,*]Ji Guoliang,
[1,2]School of Materials Science and Engineering, Henan Polytechnic University, Jiaozuo city, Henan Province, China
*Corresponding author

Abstract: In wind power gearbox, sliding bearings are more and more widely used in installation. By laser cladding surface modification technology, sliding bearings have been greatly improved in terms of friction, hardness, corrosion resistance and service life. However, the heat and mass transfer process in the laser cladding process cannot be observed and explored from a macroscopic perspective. Finite element method is needed to analyze the thermal cycle process in the molten pool and the solidification characteristics of the cladding layer, so as to promote the optimization of the laser cladding process parameters. Based on CuSn12Ni2 process of laser cladding on 20 steel pipes, the temperature field and flow field in the cladding process are simulated in this paper. A finite element model of the flow field considering the fluid flow in the molten pool is established, and the flow of the molten pool is simulated in the form of dynamic grid. The fluid flow rules in the molten pool under different process parameters were investigated. When considering the fluid flow in the molten pool, with the increase of cladding time, the flow field distribution tends to be stable after 0.4 s, and the fluid velocity remains at 0.00129 m/s. With the increase of laser power and the decrease of scanning speed, the heat absorbed inside the molten pool increases, which makes the convection in the molten pool strengthen, and the surface size will increase. Finally, the solidification mode of CuSn12Ni2 alloy cladding layer and the microstructure transformation characteristics of heat-affected zone of 20 steel tube matrix were investigated, and the simulation results were verified. According to the calculation of G and R of the cladding layer, the G/R value of zone A at the bottom of the cladding layer is higher, which is 24.6e9 k·s·mm^-2, showing plane crystallization. The G/R value in zone C at the top of the molten pool is 0.59e9 k·s·mm^-2, showing the coexistence of isotropic crystals and columnar dendritic crystals. The B zone in the middle of the pool with the lowest G/R value (0.06e9 k·s·mm^-2and the highest G×R value (4210.71k·s^-1) shows columnar dendritic crystals. It is found that the calculated results of G/R and G×R are in good agreement with the experimental solidification model, which verifies the correctness of the model.

Keyword： *Laser Cladding；Sliding Bearing；Flow Field；Numerical Modeling*

I. INTRODUCTION

Plain bearings are more suitable for large load and low speed working scenarios。Now plain bearings through surface modification technology has been greatly improved in terms of friction performance, hardness, corrosion resistance and service life. However, in order to reduce the cost of industrial production, the surface modification technology of plain bearings still needs to be further improved and improved。Laser cladding technology is widely popular in the process of surface modification of plain bearings. In the process of laser cladding of specified materials on the matrix, the corrosion resistance and wear resistance of the matrix have been significantly improved, so as to achieve the purpose of repairing or changing the performance of the matrix。However, in the process of laser cladding, the internal heat conduction and Marangoni flow in the molten pool determine the microstructure changes of the workpiece after forming. Laser cladding is a very uneven and instantaneous physicochemical metallurgical process,When looking for the best process parameters, if the best data are obtained through repeated experiments, the efficiency of industrial production will be limited to a certain extent, and it is difficult to observe the flow of the molten pool during the laser cladding process. Researchers are increasingly using finite element methods (FEM) to narrow the material processing window, thereby reducing the high cost of testing large numbers of samples[1]。Therefore, the finite element simulation technology was used to simulate the laser cladding process, and the distribution law of temperature field and flow field in the melting pool was studied，It can provide an effective theoretical basis for the actual process. It is of great significance to realize high performance laser cladding. In 2022, the United States launched a new program called "Additive Manufacturing Frontiers" (AM Forward)， The goal is to improve competitiveness among small manufacturers. Additive manufacturing technology has been heavily invested by countries all over the world, and has become an important technical means to promote national development in the manufacturing industry. Laser cladding technology is divided into four feeding methods, namely: coaxial powder feeding system, off-axis powder feeding system, preset powder system and wire feeding system[2-5].The coating material absorbs the high density energy emitted by the laser source and melts at the same time with the substrate surface, or only the coating material melts and spreads on the substrate surface to form a melt pool. After the laser beam leaves, the melt pool solidifies rapidly to form a coating with low dilution rate, good wear resistance and corrosion resistance.Figure 1 shows the principle diagram of laser cladding wire feeding system and coaxial powder feeding system.

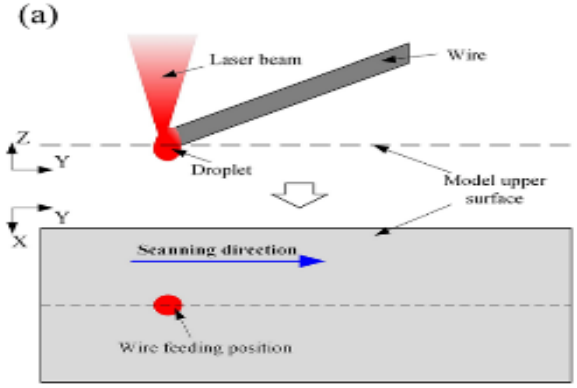

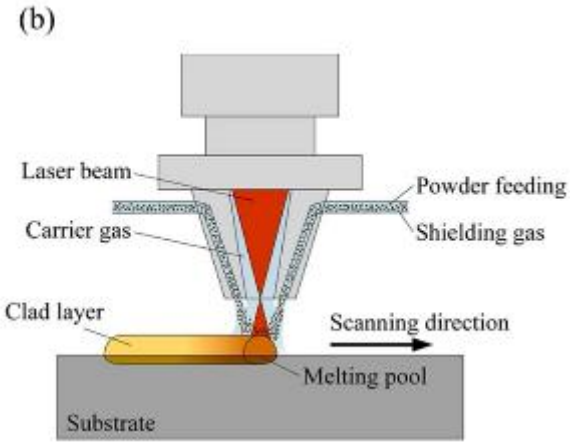

Fig.1. Schematic diagram of laser cladding[6, 7]**:**(a) wire feed system;(b)coaxial powder feeding system

XingHanet al[8] think laser cladding is a new surface modification technology,rapid heating of the workpiece can be achieved. The crystal structure of the molded parts obtained by laser cladding is fine and the dilution rate is very low. Moreover, the combination strength of the finished workpiece is high, and the range of heat affected zone is small, which can meet the process requirements well. At the same time, a multi-field coupling model is established on the surfacing layer. The experimental results show that laser cladding can make up for the defects in the surfacing welding process and improve the surface quality of the substrate. Figure 2 shows the composite process diagram of surfacing welding and laser cladding.

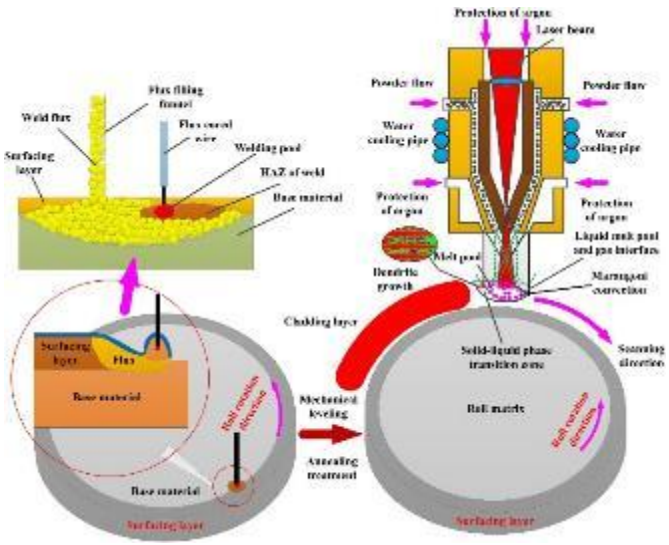

Fig.2 Composite process diagram of surfacing welding and laser cladding[9]

Boxue Songat al[10] constructed a numerical model of non-plane laser cladding for V-shaped slots with different drawing angles to explore the working mechanism of non-plane laser cladding and the influencing factors of cladding quality; The final calculation results show that the oscillatory expansion stage at the bottom of the V-shaped groove is very similar to the planar laser cladding process, and both of them are in periodic steady state at last. Lipeng Wangat al[11]based on finite element method, the numerical model of laser cladding of crankshaft journal is established. Fe45 powder was laser-coated on ASTM1045 substrate by a disk laser. The evolution model of the grains during solidification was established, and the morphology and size of the grains distributed in the cladding layer were analyzed. The accuracy of the model is verified by comparing the microstructure characteristics with the experimental results. In the process of laser cladding, the quality of cladding layer is directly affected by laser power, scanning speed and other parameters. The laser power will affect the input energy of the laser source to the molten pool in unit time, and then affect the quality of the laser cladding molding[12];The scanning speed will affect the residence time of the laser source in the matrix, which will affect the height of the cladding layer and the formation of pores and other defects in the cladding layer. The thermal cycle in laser cladding process is an important factor affecting the coating quality and properties[13, 14].In the simulation, it is necessary to consider not only the processing parameters such as laser power and scanning speed, but also the processing environment and the material properties of the wire. In recent years, with the rapid development of computer technology, the simulation of laser cladding process has become more and more accurate and efficient, and more and more researchers have optimized the laser cladding process through simulation technology.

In 2017, Gan Zhengtao [15]The numerical model of laser cladding was established, and the temperature field, flow field and solidification changes were studied. However, the effect of temperature change on physics does not take into account the properties of substrate and powder particles, and the attenuation of powder particles to laser energy is ignored.Figure 3 shows the simulated temperature field distribution cloud map.

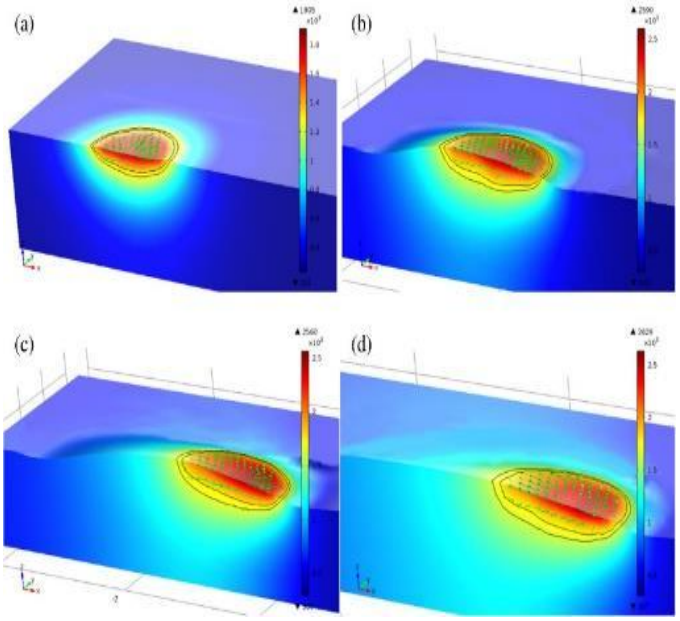

Fig.3 Cloud picture of temperature field distribution at different time：(a) 10ms；(b)300ms；(c)500ms；(d)700ms

FlorianWirth at al[16] established a three-dimensional finite element simulation model of laser cladding process considering thermal effects. The improved height function method is used to calculate the surface profile.The model was implemented by COMSOL Multiphysics, a commercial finite element software. The model has high prediction ability, especially the prediction ability of heat input. YueweiAi at al established a 3D numerical model to analyze the molten metal behavior and the formation process of cladding layer in laser additive manufacturing with 316L stainless steel wire; Finally, the flow field of the calculated results is analyzed and discussed. It is found that the molten metal is periodically transported to the molten pool in droplet form along the 316L

stainless steel wire, and then gradually solidifies into a cladding layer with corrugated surface[17].Figure 4 shows the flow field distribution in the simulation results.

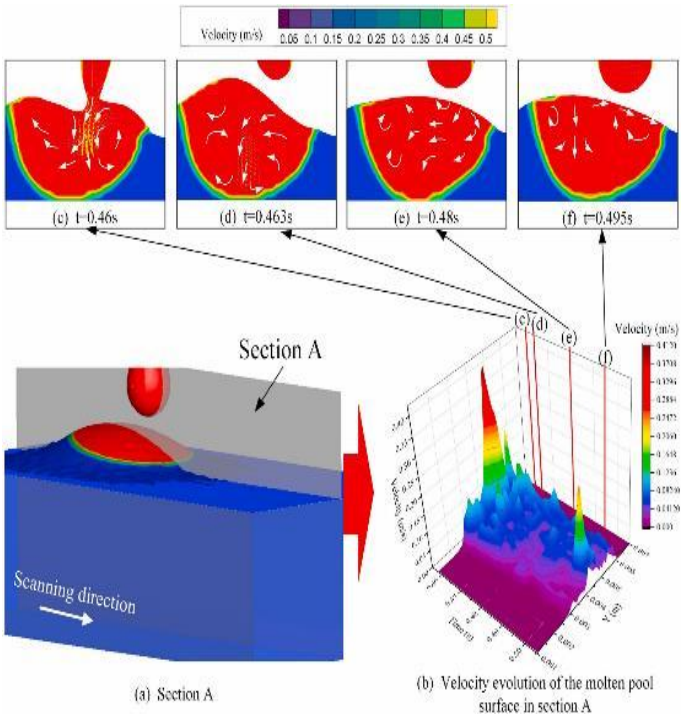

Fig.4 Flow field distribution at different times

ChangLiat al[18]established the mathematical model of Fe60 powder coating on ASTM1045 substrate. In the model, CALPHAD software is first used to calculate the necessary thermal physical performance parameters of the model and input them into the model, and then the boundary conditions are set and solved. The results show the shape of the cladding layer corresponding to each time, and the influence of the surface tension and laser energy on the liquid flow of the molten pool is analyzed. Finally, the correctness of the simulation is verified by comparing with the experiment.In this paper, the finite element method is used to simulate the CuSn12Ni2 laser cladding process on the surface of 20 steel pipes. The finite element model of laser cladding was constructed by using dynamic grid method when fluid flow in molten pool was considered. The fluid distribution in the flow field and the influence of different process parameters on the flow field were investigated. The influence of flow field on temperature field is analyzed.

II. FINITE ELEMENT MODEL SETTING

A. Material thermal property parameter setting

At present, the widely used material for the electric gear shaft in the market is 20 steel, and the substrate material in this process is 20 steel plain bearing. As a very excellent cladding material for wind power gear shaft, copper alloy is very prominent compared with other alloys in terms of wear resistance, high temperature resistance and self-lubricating surface, so it is often used as a wear reduction coating for workpieces in industry. Due to the actual process requirements, the cladding layer is made of CuSn12Ni2 wire. Table 1 shows the composition of 20 steel materials, and Table 2 shows the composition of CuSn12Ni2 materials. The thermodynamic calculation of the two metals was carried out using the calculation software of the calculation principle of equilibrium phase diagram, and the thermodynamic properties of steel 20 and CuSn12Ni2 wire were obtained, as shown in Figure 5. Due to the need to study the molten pool fluid in this paper, the relevant properties of the fluid are calculated. Through calculation, the melting point of the CuSn12Ni2 wire is 600 ℃, and the liquidus temperature is 890 ℃. The solid-liquid diagram of the wire and the fluid viscosity are shown in Figure 6. The viscosity of the fluid is used to calculate the flow field of the molten pool.

Table 1: 20 Composition of steel materials

C	Si	Mn	P	S	Ni	Cr
0.17~0.23	0.17~0.37	0.35~0.65	<=0.035	<=0.035	<=0.30	<=0.25

Table 2 Components of CuSn12Ni2

Cu	Sn	Al	Fe	Mn	Ni	Pb	Si	P
86.7	11.4	<0.005	0.008	<0.005	1.74	<0.005	<0.05	0.11

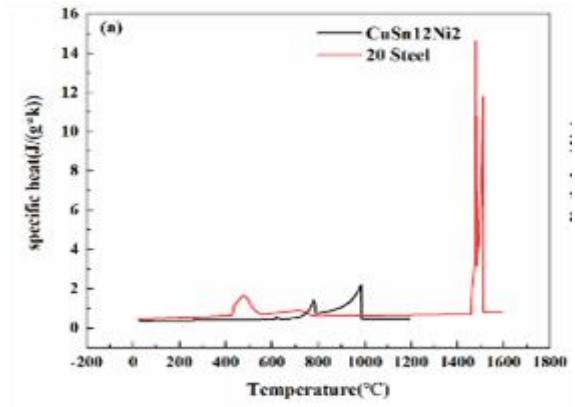

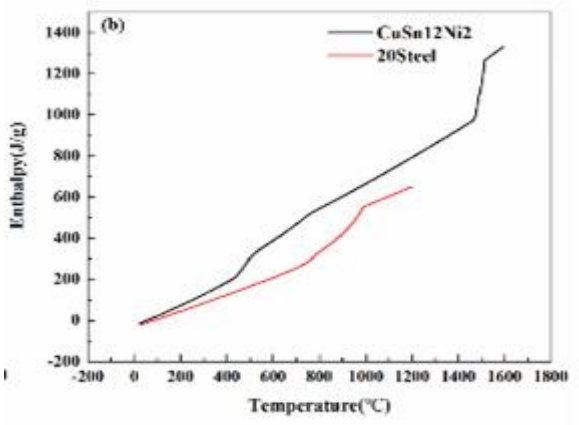

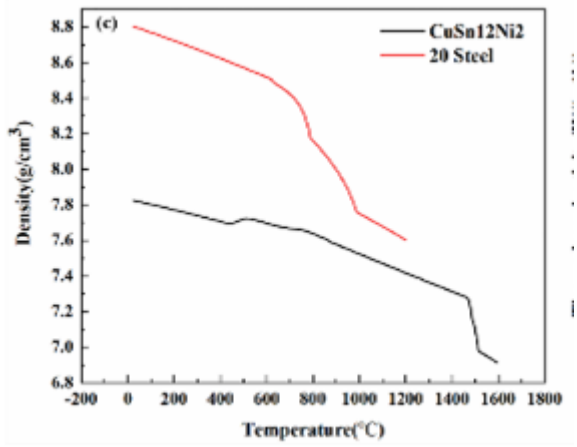

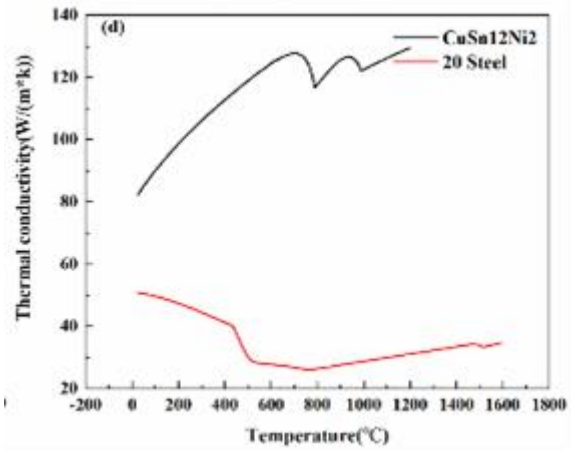

Fig. 5 Thermodynamic properties of steel 20 and CuSn12Ni2: (a) specific heat; (b) enthalpy change; (c) Density; (d) Coefficient of thermal expansion

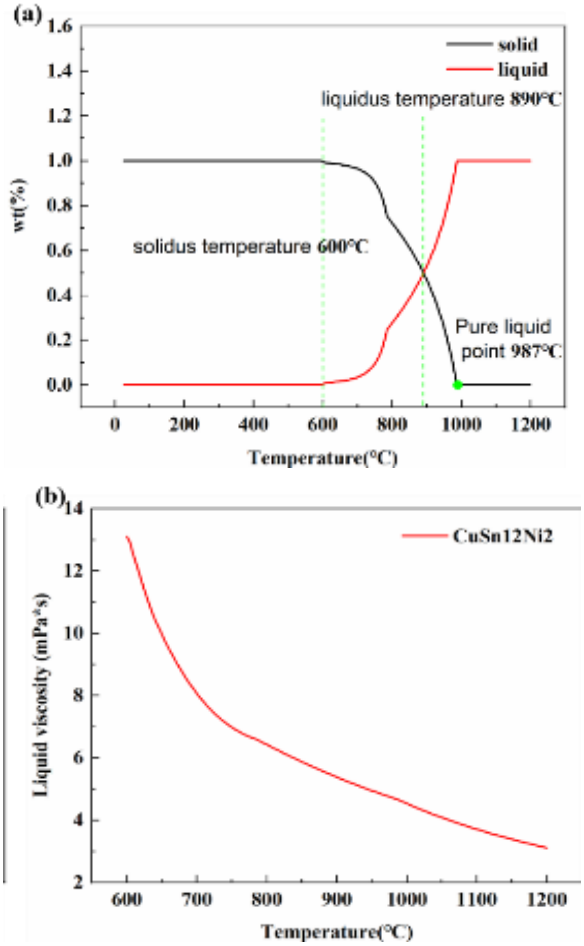

Fig.6 Related thermal physical properties of the fluid: (a) CuSn12Ni2 solid-liquid phase diagram; (b) CuSn12Ni2 fluid viscosity

B. Finite element model building

Laser cladding involves many physical processes, such as heat convection and heat conduction. If you want to conduct in-depth research on these physical processes, then it is necessary to analyze and study the physical phenomena generated during the laser cladding process. Then, according to the need to simplify the research problem and model and put forward the necessary assumptions, and finally use partial differential equation and other mathematical methods to calculate and describe these physical phenomena.

1. It is assumed that the thermophysical parameters of matrix and cladding material change with the change of temperature;
2. It is assumed that the cladding material and the substrate are isotropic and uniform;
3. It is assumed that the heat source model applied to the surface of the cladding layer is a compound heat source combined with the Gaussian surface heat source and the cylinder heat source;
4. It is assumed that the cladding layer is a continuous medium in solid, liquid or gas state;
5. Assuming that the fluid in the molten pool is an uncompressed laminar flow liquid, the driving force of the molten liquid ignores the influence of buoyancy, and only considers the surface tension coefficient and gravity.

In order to explore the influence of laser cladding flow field on the entire laser cladding process, it is necessary to re-establish the model and make grid division and model assumptions. In order to simplify the model, only the influence of surface tension and gravity on fluid flow in the molten pool is considered, and the influence of arc force and buoyancy on the molten pool is ignored.Figure 7 shows the grid division diagram of the flow field model. The model is still cladding CuSn12Ni2 alloy on the surface of 20 steel tubes with a diameter of 300 mm and a width of 400 mm. The cladding coating area on the substrate surface is set as a refined free tetrahedral mesh. In order to more closely resemble the molten pool configuration, grid cells were established at intervals of 0.5 mm. To save calculation time, the other parts are set as a coarse-free tetrahedral grid. The computing domain contains 302,744 domain units, 99,168 boundary units, and 2364 edge units. Other parameters are consistent with those of temperature field modeling.

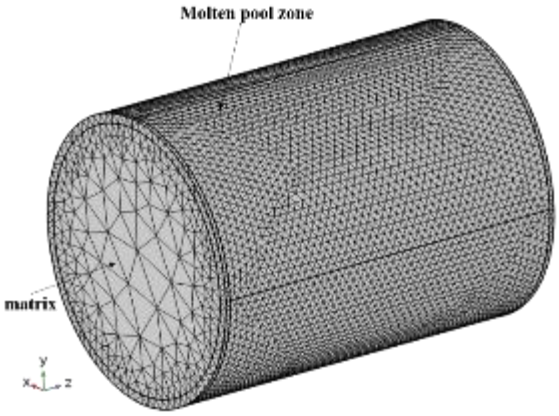

Fig.7 Finite element model fluid modeling grid division

C. Fluid flow governing equations and boundary conditions

Mass transport, heat transfer and fluid flow in molten pool are controlled by mass conservation, energy conservation and momentum equations:(1) Is the mass conservation equation,(3) Is the energy conservation equation,(4) Is the momentum conservation equation.

$$\frac{\partial \rho}{\partial t} + \nabla \cdot (\rho \vec{v}) = \mathrm{M}_s \#(1)$$

In the formula：ρ——material density（g/cm^3）；

$\vec{v}$——the velocity vector of the fluid（m/s）；

∇——divergence of expression.

thereinto$\nabla.(\rho\vec{v})$satisfy the following relation：

$$\nabla.(\rho\vec{v}) = \frac{\partial(\rho u_0)}{\partial_x} + \frac{\partial(\rho v_0)}{\partial_y} + \frac{\partial(\rho w_0)}{\partial_z} \#(2)$$

In the formula： u_0、v_0、w_0 represents the velocity components in the x, y, and z axes, respectively（m/s）。

$$\rho\frac{\partial T}{\partial t} + \rho\vec{v}.\nabla T = \nabla.(\mathrm{k}\nabla\mathrm{T}) + S_H \#(3)$$

In the formula：T——temperature of material（K）;

K——thermal conductivity of the material（W/m· K）

S_H——energy source term.

$$\rho\left[\frac{\partial\vec{V}}{\partial t} + \vec{V}\cdot\nabla\vec{V}\right] = \mu\nabla^2\vec{V} - \nabla p + M_s\cdot\vec{V} + F \#(4)$$

In the formula：μ is the dynamic viscosity of liquid metal，P is pressure，F represents the force on the solid-liquid two phases in the molten pool, including thermal capillary force, viscous resistance, gravity, etc. In the laser cladding process, the first phase transition process of the wire is the melting of a solid into a liquid in the molten pool. This process is accompanied by heat transfer within and between phases, and according to the enthalpy-porosity technique, the definition of liquid phase fraction β is used to determine the pure solid phase, the pure liquid phase and the viscous region[19]。

$$\beta = \begin{cases} 0 & \mathrm{T} < \mathrm{T_S} \\ \dfrac{\mathrm{T}-\mathrm{T_S}}{\mathrm{T_L}-\mathrm{T_S}} & \mathrm{T_S} \le \mathrm{T} \le \mathrm{T_L} \\ 1 & \mathrm{T_L} < T \end{cases} \#(5)$$

At this time, the total enthalpy value of the material H conforms to the following formula[20]。

$$\mathrm{H} = \mathrm{cT} + \beta\mathrm{L} \#(6)$$

Where, c is specific heat, L is latent heat of liquefaction, $\mathrm{T_S}$ and $\mathrm{T_L}$ respectively are the solid-phase line temperature and liquidus temperature. Natural convection refers to the convection heat transfer between the matrix, the molten pool and the outside world in the natural state, and the flow generated by the liquid phase pair of the molten metal without external forces. The existence of natural convection can drive the uniform distribution of various elements in the molten pool. Because the temperature rise will gradually reduce the density of the metal wire, and the newly molten metal liquid phase is heavier, and the lighter metal liquid will flow to the top of the molten pool. This cyclic process constitutes natural convection in the molten pool. The boundary conditions (convective heat dissipation conditions) of other areas except the heat source area on the upper surface of the melting pool are as follows:

$$-\mathrm{k}\frac{\partial\mathrm{T}}{\partial\mathrm{z}} = \mathrm{q} - \mathrm{h_c}(\mathrm{T}-\mathrm{T_0}) - \sigma\varepsilon(\mathrm{T}^4 - \mathrm{T_0^4}) \#(7)$$

Other surface (side) boundary conditions are as follows:

$$-\mathrm{k}\frac{\partial\mathrm{T}}{\partial\mathrm{n}} = -\mathrm{h_c}(\mathrm{T}-\mathrm{T_0}) - \sigma\varepsilon(\mathrm{T}^4 - \mathrm{T_0^4}) \#(8)$$

In the formula:T——surface temperature（℃）;

h_c——is the convective heat transfer coefficient（W/m^2 ·℃）;

T_0——environment temperature（℃）;

σ——Stephen Boltzmann constant;

ε——The emissivity of the material surface.

Because the time of forming molten pool in laser cladding process is very short, it cannot be monitored and measured in real time. The flow of metal liquid in the molten pool is caused by the Marangoni flow, which triggers mass transfer in the molten pool.The principle of the Marangoni effect is that in the process of laser cladding, the fluid moves relative to each other due to the difference in surface tension at the interface of two fluids[21].The temperature difference of the molten liquid surface leads to the difference of the surface tension gradient, which makes the flow of the fluid on the surface and inside the molten pool unbalanced. The surface tension of the molten pool is expressed as follows:

$$\gamma = \gamma_0 - \sigma(\mathrm{T}-\mathrm{T_0}) \#(9)$$

In the formula：σIs the surface tension coefficient;γ_0Is the surface tension at the reference temperature T0; The boundary conditions on the molten pool surface are:

$$\begin{cases} y = 0 \\ v = 0 \\ \mu\dfrac{\partial w}{\partial y} = -\dfrac{\partial T}{\partial z}\times\dfrac{\partial\sigma}{\partial T} \\ \mu\dfrac{\partial u}{\partial y} = -\dfrac{\partial\sigma}{\partial T}\times\dfrac{\partial T}{\partial x} \end{cases} \#(10)$$

In the formula：μ is viscosity，$\frac{\partial\sigma}{\partial T}$is the temperature coefficient of surface tension.

D. Flow field distribution of molten pool

The process parameters used in this simulation are as follows: laser power 4000 W, scanning speed 20 mm/s, wire feed rate 40 mm/s.When fluid flow in the molten pool is considered, the maximum velocity of fluid in the longitudinal section of the molten pool varies with time as shown in Figure 8. It can be seen from the figure that the flow field distribution tends to be stable after 0.4s, and the fluid velocity remains at about 0.00129m /s. The reason for this phenomenon is that the initial cladding time is short, the melting pool has just begun to form, and the matrix heat has not accumulated to a certain extent. With the passage of time, the heat absorption of the molten pool increases, and the fluid flow rate of the molten pool increases continuously until it reaches a stable value.

It can be seen from the hypothesis that the driving force of the fluid in the molten pool is surface tension gradient and gravity. Under these two driving forces, the fluid on the upper surface of the molten pool flows to both ends. As the molten metal drops onto the substrate, the cladding layer continues to rise, and the fluid flowing to the two ends produces a height difference; This height difference makes the fluid flow to the bottom of the molten pool, and then the molten metal at the bottom flows to the middle of the molten pool. After flowing to the middle of the molten pool, the liquid metal is squeezed by the fluid on both sides of the molten pool, making the liquid metal flow upward to the surface of the molten pool.Fig. 9 is the superposition cloud image of the temperature velocity vector of the molten pool, where the arrow represents the direction of fluid flow. From the cloud image of the upper surface of the molten pool, it can be seen that the distribution

of the molten pool is circular. In addition, the arrow distribution in the middle of the molten pool is sparse and the flow velocity is small, while the arrow distribution at the bottom of the molten pool is dense and the flow velocity is large, and the direction of the arrow is distributed in all directions of the ring, representing the flow of fluid in the molten pool to all directions at the bottom of the molten pool. The fluid flow velocity in the area outside the bottom of the molten pool gradually approaches 0.From the velocity vector diagram of the cross section of the molten pool, it can be seen that the molten metal flows from the upper surface of the molten pool to the bottom of the molten pool, and then flows to the upper surface of the molten pool after the fluid is squeezed. This is because there is a large temperature gradient in the center of the molten pool, and the liquid flow rate of the molten pool is affected by the Marangoni flow, so that the molten metal liquid in the molten pool forms such a circulating eddy.

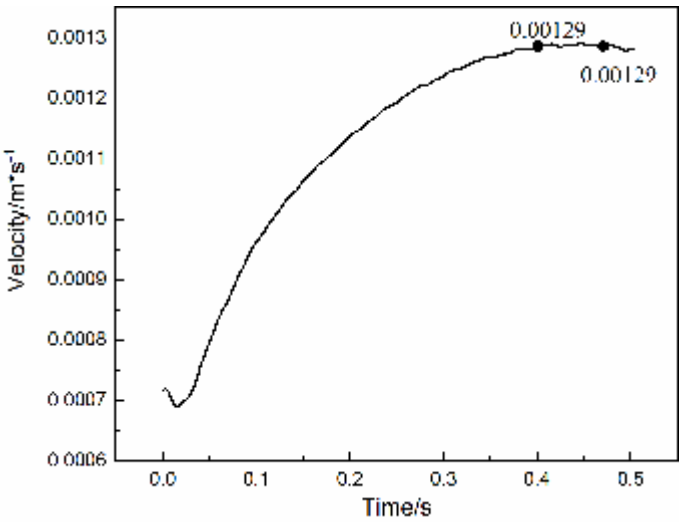

Fig.8 Variation of maximum fluid velocity in longitudinal section of molten pool with time

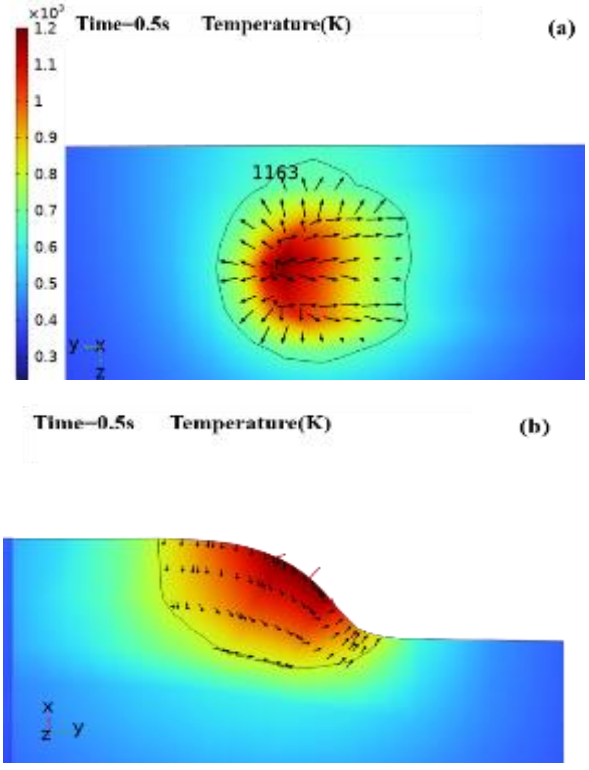

Fig.9 Superimposed cloud diagram of temperature and velocity vector of the molten pool :(a) Velocity vector diagram of the upper surface of the molten pool; (b) velocity vector diagram of the transverse section of the molten pool

In order to explore the influence of laser power on the flow field, the laser scanning speed was set to 20 mm/s in the finite element model, and other parameters remained unchanged. Each simulation calculation only changes the laser power size, and the laser power is 4000 W and 5000 W respectively. Figure 10 shows the cloud image of the longitudinal cross-section shape of the molten pool at different powers. It can be seen from the flow arrow distribution in the figure that the size of the molten pool and the fluid flow velocity in the molten pool increase with the increase of laser power when the scanning speed is constant. When the power increases, the convection effect of the fluid in the molten pool is enhanced, because the heat conduction effect of the fluid in the molten pool is enhanced with the increase of the laser power.

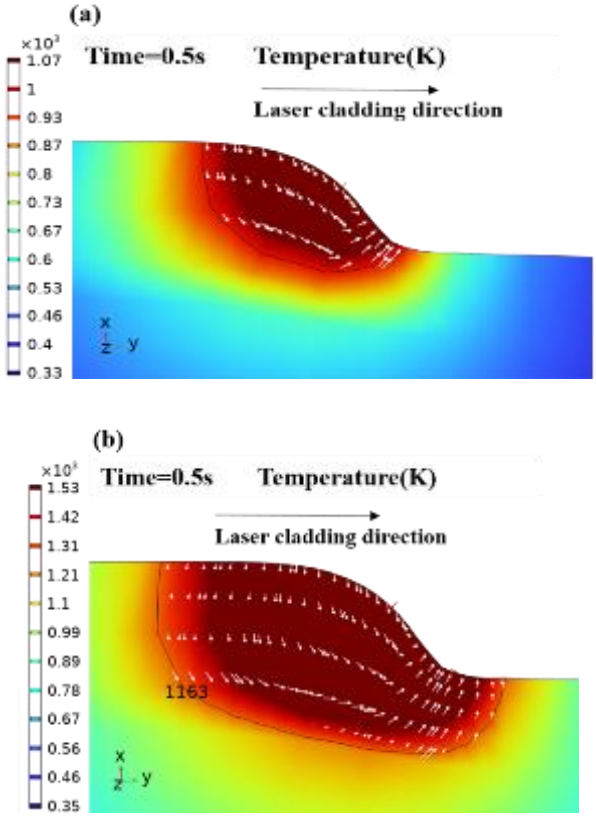

Fig. 10 Cloud diagram of molten pool shape under different power: (a) 4000w; (b) 5000w

In addition to the laser power, the laser scanning speed also affects the flow of fluid in the molten pool. FIG. 11 shows the flow velocity diagram of the molten pool longitudinal section at a scanning speed of 21.42 mm/s and 16.83 mm/s at a laser power of 4000 W for 1s. By comparing the figures in FIG. 11, it can be seen that the longitudinal size of the molten pool increases as the scanning speed decreases. In addition, the convection effect on the right side eddy current is stronger with the decrease of scanning speed. This is because the decrease of scanning speed will cause the heat accumulation in the molten pool, the temperature difference will increase, and the convection effect will be enhanced, so the right eddy current convection will be enhanced. Both the laser scanning speed and the laser power in essence change the absorbed laser energy in the molten pool to affect the fluid velocity in the molten pool. The microstructure of the cladding layer and the properties of the cladding parts are changed.

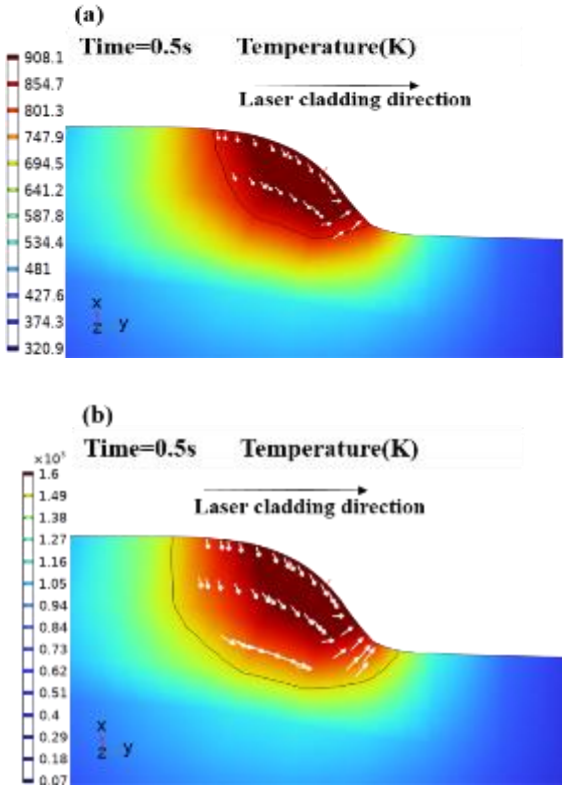

Fig. 11 Shape of molten pool at different scanning speeds：(a) 21.42 mm/s；(b) 16.83mm/s

E. Study on solidification characteristics of cladding layer

Two important data, temperature gradient G and solidification rate R, can be used to analyze the microstructure during solidification. Where G×R determines the size of the microstructure in the solidification process, which is called the size factor. The higher the G×R, the finer the microstructure. G/R determines the morphology of the microstructure, that is, the morphology changes of planar crystals, cellular crystals, columnar dendrites and equiaxial crystals are shown in Figure 12[22]. The temperature gradient G and solidification rate R are the key factors that determine the microstructure characteristics. The G and R expressions are shown in equation 11[23, 24].

$$\begin{cases} G = \dfrac{\Delta T_d}{\Delta d} \\ R = \dfrac{1}{G} \times \dfrac{\partial T}{\partial t} \end{cases} \#(11)$$

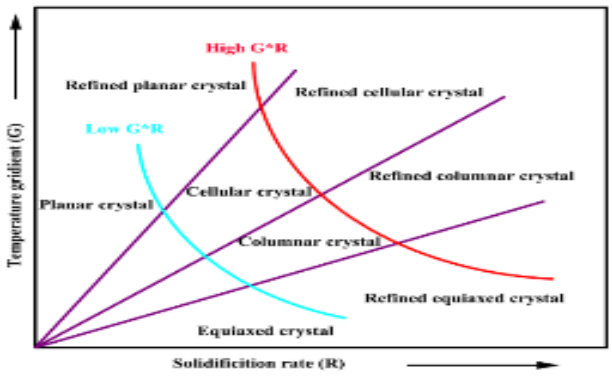

Fig. 12 Relationship between G and R

FIG. 13 shows the microstructure diagram of the cladding layer. It shows that the G/R value in zone A at the bottom of the molten pool is high, which is 24.6e9 k·s·mm^-2, while the G×R value is low, which is 4110 k/s, showing planar crystallization. At the top of the molten pool, the G/R value in zone C is low (0.59e9 k·s·mm^-2, and the G×R value is high (4115 k/s), showing the coexistence of isotropic crystals and columnar dendritic crystals. The B region with the lowest G/R value (0.06e9 k·s·mm^-2) and the highest G×R value (4210.71 k/s) appears as columnar dendritic crystals. The calculated results of G/R and G×R are in good agreement with the experimental results, which verifies the correctness of the model.

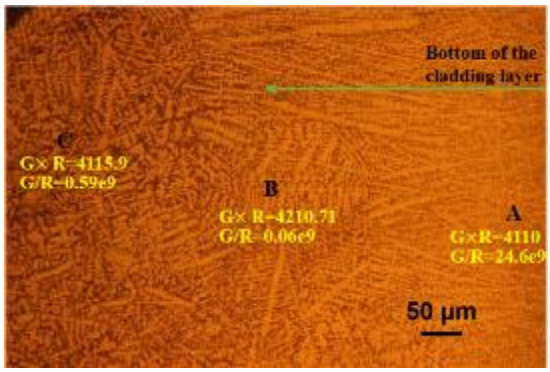

Fig. 13 Microstructure of cladding layer

Figure 14 shows the temperature distribution in the heat affected zone. Through the comparison of microstructure and temperature distribution, it can be found that the width of the heat affected zone is roughly 150 um, but there are still some differences in other positions. The difference between the experimental results and the simulated results may be attributed to the following factors: the finite element model of laser cladding does not take into account the fluid flow in the molten pool, and the width of the heat affected zone is random due to various process factors.

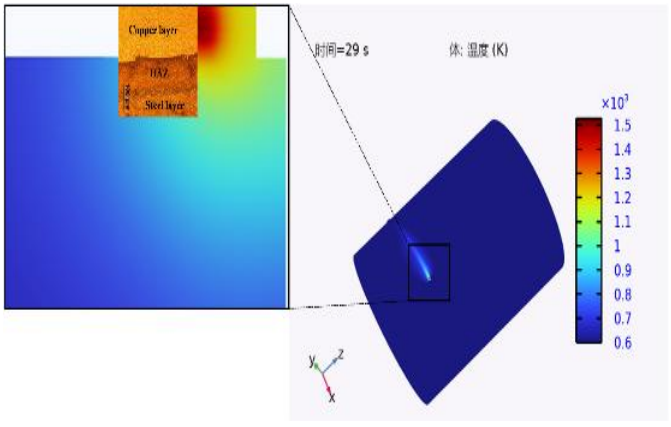

Fig. 14 Comparison of simulated and actual measured HAZ widths

CONCLUSION

Based on the actual process parameters of laser cladding CuSn12Ni2 on the surface of No. 20 steel pipe, a finite element model was established to calculate the fluid flow state of the molten pool. Through the analysis of the calculation results, the solidification mode of CuSn12Ni2 alloy cladding layer and the microstructure transformation characteristics of the heat-affected zone of No. 20 steel tube matrix are revealed, and the accuracy of the simulation is verified. The main conclusions are as follows:

（1）When considering the fluid flow in the molten pool, with the increase of cladding time, the flow field distribution

tends to be stable after 0.4s, and the fluid velocity remains at 0.00129m /s. With the increase of laser power and the decrease of scanning speed, the heat absorbed inside the molten pool increases, which makes the convection in the molten pool strengthen, and the surface size will increase.

（2）According to the calculation of G and R of the cladding layer, the G/R value of zone A at the bottom of the cladding layer is higher, which is 24.6e9 k·s·mm^-2, showing plane crystallization. At the top of the molten pool, the G/R value in zone C is low, which is 0.59e9 k·s·mm-2, showing the coexistence of isotropic crystals and columnar dendritic crystals. The middle B zone of the cladding layer with the lowest G/R value (0.06e9k·s·mm^-2) and the highest G×R value (4210.71k·s-1) shows columnar dendritic crystals. It is found that the calculated results of G/R and G×R are in good agreement with the experimental solidification model, which verifies the correctness of the model.

References

[1] Liang-Xing Lu, N. Sridhar, ZHANG Y. Phase field simulation of powder bed-based additive manufacturing[J]. Acta Materialia, 2018,144: 801-809.

[2] ZHU L, XUE P, LAN Q. Recent research and development status of laser cladding: A review [J]. Optics and Laser Technology, 2021,136.

[3] LIU I, YU H, CHEN C. Research and development status of laser cladding on magnesium alloys: A review[J]. Optics and Lasers in Engineering, 2017,93: 195-210.

[4] FARNIA A, GHAINI F M, SABBAGHZADEH J. Effects of pulse duration and overlapping factor on melting ratio in preplaced
pulsed Nd:YAG laser cladding[J]. Optics and Lasers in Engineering, 2013,51: 69-76.

[5] HOFMAN J T, de LANGE D F, PATHIRAJ, et al. FEM modeling and experimental verification for dilution control in laser cladding[J]. Journal of Materials Processing Technology, 2011,211(2).

[6] SUN Z, CHEN L, CHEN X, et al. Analysis and prediction of Cu-Sn-Ti alloy deposited on 316 L steel by coaxial laser cladding[J]. Optik, 2023,282: 170839.

[7] AI Y, WANG Y, HAN S, et al. Investigation of cladding layer formation in uphill wire feeding laser additive manufacturing on inclined substrate[J]. Applied Thermal Engineering, 2024: 122919.

[8] HAN X, LI C, CHEN X, et al. Numerical simulation and experimental study on the composite process of
submerged arc cladding and laser cladding[J]. Surface & Coatings Technology, 2022,439.

[9] HAN X, LI C, CHEN X, et al. Numerical simulation and experimental study on the composite process of submerged arc cladding and laser cladding[J]. Surface & coatings technology, 2022,439: 128432.

[10] A B S, TIANBIAO Y A, JIANG X, et al. Evolution and convection mechanism of the melt pool formed by V-groove laser cladding [J]. Optics and Laser Technology, 2021,144.

[11] WANG L, ZHANG D, CHEN C. Multi-physics field coupling and microstructure numerical simulation of laser cladding for engine crankshaft based on CA-FE method and experimental study [J]. Surface & Coatings Technology, 2022,438.

[12] YE W, SUN A, ZHAI W, et al. Finite element simulation analysis of flow heat transfer behavior and molten pool characteristics during 0Cr16Ni5Mo1 laser cladding[J]. Journal of Materials Research and Technology, 2024,30: 2186-2199.

[13] VUNDRU C, PAUL S, SINGH R, et al. Numerical analysis of multi-layered laser cladding for die repair applications to determine residual stresses and hardness[J]. Procedia Manufacturing, 2018,26: 952-961.

[14] TAMANNA N, KABIR I R, NAHER S. Thermo-mechanical modelling to evaluate residual stress and material compatibility of laser cladding process depositing similar and dissimilar material on Ti6Al4V alloy[J]. Thermal Science and Engineering Progress, 2022,31: 101283.

[15] ZHENGTAO GAN G Y X H. Numerical simulation of thermal behavior and multicomponent mass transfer in direct laser deposition of Co-base alloy on steel,[J]. International Journal of Heat and Mass Transfer, 2017,104: 28-38.

[16] WIRTH F, WEGENER K. A physical modeling and predictive simulation of the laser cladding process[J]. Additive Manufacturing, 2018,22.

[17] AI Y, YAN Y, YUAN P, et al. The numerical investigation of cladding layer forming process in laser additive manufacturing with wire feeding[J]. International Journal of Thermal Sciences, 2024,196: 108669.

[18] LI C, YU Z, GAO J. Numerical simulation and experimental study of cladding Fe60 on an ASTM
1045 substrate by laser cladding[J]. Surface & Coatings Technology, 2019,357: 965-977.

[19] KAN X, YIN Y, YANG D, et al. Micro pool characteristics of 316L and the influence of sulfur during SLM[J]. Optics & Laser Technology, 2021,142: 107136.

[20] LYU P, LI P, JIANG K. Numerical simulation and experimental investigation of the laser cladding processes of Ti6Al4V with coaxial shroud protection[J]. Journal of Materials Research and Technology, 2023,26: 4133-4150.

[21] AL-MDALLAL Q M, INDUMATHI N, GANGA B, et al. Marangoni radiative effects of hybrid-nanofluids flow past a permeable surface with inclined magnetic field[J]. Case Studies in Thermal Engineering, 2020,17: 100571.

[22] LI C, YU Z B, GAO J X, et al. Numerical simulation and experimental study on the evolution of multi-field coupling in laser cladding process by disk lasers[J]. Welding in the World, 2019,63(4): 925-945.

[23] SONG B, YU T, JIANG X, et al. Development mechanism and solidification morphology of molten pool generated by laser cladding[J]. International Journal of Thermal Sciences, 2021,159: 106579.

[24] CHEN C, MEIPING W, RUI H, et al. Understanding Stellite-6 coating prepared by laser cladding: Convection and columnar-to-equiaxed transition[J]. Optics & Laser Technology, 2022,149: 107885.